ELSEVIER

π^0 Photo- and electroproduction at threshold within a dynamical model

S.S. Kamalov [a,1], Guan-Yeu Chen [a], Shin Nan Yang [a], D. Drechsel [b], L. Tiator [b]

[a] *Department of Physics, National Taiwan University, Taipei, 10764 Taiwan, ROC*
[b] *Institut für Kernphysik, Universität Mainz, 55099 Mainz, Germany*

Abstract

We show that, within a meson-exchange dynamical model describing most of the existing pion electromagnetic production data up to the second resonance region, one is also able to obtain a good agreement with the π^0 photo- and electroproduction data near threshold. The potentials used in the model are derived from an effective chiral Lagrangian. The only sizable discrepancy between our results and the data is in the P-wave amplitude $P_3 = 2M_{1+} + M_{1-}$ where our prediction underestimate the data by about 20%. In the case of π^0 production, the effects of final state interaction in the threshold region are nearly saturated by single charge exchange rescattering. This indicates that in ChPT it might be sufficient to carry out the calculation just up to one-loop diagrams for threshold neutral pion production.

© 2001 Elsevier Science B.V. Open access under CC BY license.

Chiral perturbation theory (ChPT) provides us with a systematic scheme to describe the low energy interactions of Goldstone bosons among themselves and with other hadrons, because it is based on a low energy effective field theory respecting the symmetries of QCD, in particular, chiral symmetry. There is generally good agreement between the ChPT predictions and experiments [1]. One case which has been very intensively studied is π^0 electromagnetic production of neutral pions near threshold where very precise measurements [2–8] have been performed and the ChPT calculation to one loop $O(p^3)$ ($O(p^4)$ in the case of photoproduction) has been carried out in the heavy baryon formulation [9,10]. Nice agreement between theory and experiment was reached not only for the S-wave multipoles E_{0+} and L_{0+} but for the P-wave amplitudes [8,10] as well.

As in ChPT, meson-exchange models also start from an effective chiral Lagrangian. However, they differ from ChPT in the approach to calculate the scattering amplitudes. In ChPT, crossing symmetry is maintained in the perturbative field-theoretic calculation, and the agreement with low energy theorems and the data is to be expected as long as the series is well convergent. In meson-exchange models, the effective Lagrangian is used to construct a potential for use in the scattering equation. The solutions of the scattering equation will include rescattering effects to all orders and thereby unitarity is ensured, while crossing symmetry is violated. Such models [11–17] have been able to provide a good description of πN scattering lengths and phase shifts in S-, P-, and D-waves up to 600 MeV pion laboratory kinetic energy.

E-mail address: snyang@phys.ntu.edu.tw (S.N. Yang).

[1] Permanent address: Laboratory of Theoretical Physics, JINR Dubna, 141980 Moscow region, Russia.

Meson-exchange models have been constructed for pion electromagnetic production as well [15,18–21] and good agreement with the data has also been achieved up to 1300 MeV total πN c.m. energy. However, the predictive power of the meson-exchange model for electromagnetic pion production near threshold has not been fully explored even though the importance of final state interaction (FSI) for threshold π^0 photoproduction had been demonstrated in several dynamical model studies [12,22–24] prior to one-loop calculations of ChPT [9].

In this Letter we will use the dynamical model (DM) recently developed in Ref. [25] where the dominant FSI effects in the nonresonant contributions at threshold are evaluated using the πN meson-exchange model developed in Ref. [13]. Contributions which are related to the excitation of resonances are considered phenomenologically using standard Breit–Wigner forms. In our previous work [25] such an approach gives an excellent description of pion photo- and electroproduction in the first resonance region. Here we apply this model to these reactions in the threshold region and compare our predictions with the recent experimental data [3–8] for the S- and P-wave multipoles and cross sections, and with the result of ChPT.

In the dynamical model for pion photo- and electroproduction [26,27], the t-matrix is given as

$$t_{\gamma\pi}(E) = v_{\gamma\pi} + v_{\gamma\pi} g_0(E) t_{\pi N}(E), \qquad (1)$$

where $v_{\gamma\pi}$ is the $\gamma\pi$ transition potential, g_0 and $t_{\pi N}$ are the πN free propagator and t-matrix, respectively, and E is the total energy in the c.m. frame. In the present study, the matrix elements $t_{\pi N}$ are obtained in a meson-exchange πN model [13] constructed in the Bethe–Salpeter formalism and solved within Cooper–Jennings reduction scheme [28]. Both $v_{\pi N}$ and $v_{\gamma\pi}$ are derived from an effective Lagrangian containing Born terms as well as ρ- and ω-exchange in the t-channel [29,30]. For pion electroproduction we restore gauge invariance by the substitution,

$$J_\mu \to J_\mu - k_\mu \frac{k \cdot J}{k^2}, \qquad (2)$$

where J_μ is the electromagnetic current corresponding to the background contribution of $v_{\gamma\pi}$.

For the physical multipoles in channel $\alpha = \{l, j\}$, Eq. (1) gives [27]

$$
\begin{aligned}
&t_\alpha(q_E, k) \\
&= \exp(i\delta_\alpha)\cos\delta_\alpha \\
&\quad \times \left[v_\alpha(q_E, k) + P \int_0^\infty dq' \frac{R_\alpha(q_E, q') v_\alpha(q', k)}{E(q_E) - E(q')} \right],
\end{aligned}
$$
$$(3)$$

where δ_α and R_α are the πN phase shift and reaction matrix, in channel α, respectively, q_E is the pion on-shell momentum and $k = |\mathbf{k}|$ the photon momentum. In order to ensure the convergence of the principal value integral, we introduce a dipole-like off-shell form factor characterizing the finite range aspect of the potential, $f(q, q_E) = (\Lambda^2 + q_E^2)^2/(\Lambda^2 + q^2)^2$. The value for the cut-off parameter, $\Lambda = 440$ MeV, was obtained in our previous work from an analysis of the $\Delta(1232)$ resonance multipole $M_{1+}^{(3/2)}$ over a wide energy range.

For π^0 photoproduction, we first calculate the multipole E_{0+} near threshold by solving the coupled channels equation within a basis with physical pion and nucleon masses. The coupled channels equation leads to the following expression for the pion photoproduction t-matrix in the $\pi^0 p$ channel:

$$
\begin{aligned}
t_{\gamma\pi^0}(E) = {}&v_{\gamma\pi^0}(E) + v_{\gamma\pi^0}(E) g_{\pi^0 p}(E) t_{\pi^0 p \to \pi^0 p}(E) \\
&+ v_{\gamma\pi^+}(E) g_{\pi^+ n}(E) t_{\pi^+ n \to \pi^0 p}(E),
\end{aligned}
$$
$$(4)$$

where $t_{\pi^0 p \to \pi^0 p}$ and $t_{\pi^+ n \to \pi^0 p}$ are the πN t-matrices in the elastic and charge exchange channels, respectively. They are obtained by solving the coupled channels equation for πN scattering using the meson-exchange model [13]. Results for Re E_{0+} obtained from Eq. (4) are given in Fig. 1, where the FSI contributions from the elastic and charge exchange channels (second and third term in Eq. (4)), are shown by the short-dashed and dash-dotted curves, respectively, while the dotted curve corresponds to the LET results, without the inclusion of FSI. Our results clearly indicate that practically all of the final state interaction effects originate from the $\pi^+ n$ channel. Note that the main contribution stems from the principal value integral of Eq. (4).

In the coupled channels approach considered above, the $t_{\pi N}$ matrix contains the effect of πN rescattering to all orders. However, we have indeed found that only
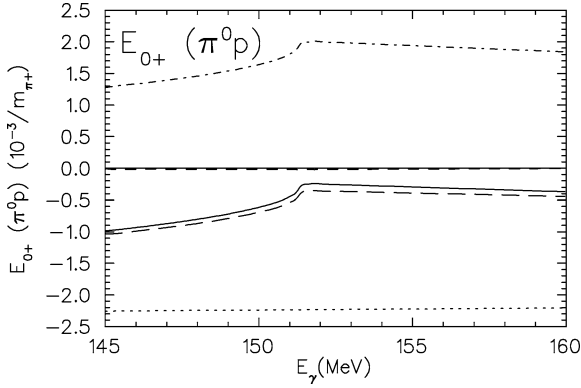
Fig. 1. Real part of the E_{0+} multipole for $\gamma p \to \pi^0 p$. The dotted curve is the result obtained without FSI, the dash-dotted and short-dashed curves are the FSI contributions from charge exchange $\pi^+ n$ and elastic $\pi^0 p$ channel, respectively. The solid and long-dashed curves are the total results (see Eq. (4)) obtained with the full matrix $t_{\pi N}$ and with $t_{\pi N}$ replaced by $v_{\pi N}$, respectively.

Fig. 2. Real (lower panel) and imaginary (upper panel) parts of the E_{0+} multipole for $\gamma p \to \pi^0 p$. The dashed and solid curves are the full results obtained without and with isospin symmetry assumption, respectively. In the latter case, the pion mass difference effect is taken into account using Eq. (5). The dash-dotted curve is the result of ChPT [10]. Data points from Ref. [3] ($\triangle$), Ref. [4] ($\bullet$), and Ref. [8] ($\circ$).

the first order rescattering contribution, i.e., the one-loop diagram, is important. This result is obtained by replacing the πN scattering t-matrix in Eq. (4) with the corresponding potential $v_{\pi N}$. As can be seen in Fig. 1, the thus obtained results given by the long-dashed curve, differ from the full calculation (solid curve) by 5% only. This indicates that the one-loop calculation in ChPT could be a reliable approximation for π^0 production in the threshold region.

If the FSI effects are evaluated with the assumption of isospin symmetry (IS), i.e., with averaged masses in the free pion–nucleon propagator, the energy dependence in Re E_{0+} in the threshold region is very smooth. Below π^+ threshold the strong energy dependence (cusp effect) [7,31] only appears because of the pion mass difference and, as we have seen above, is related to the coupling with the $\pi^+ n$ channel. In most calculations, the effects from the pion mass difference below the π^+ production channel are taken into account by using the K-matrix approach [10,32],

$$
\begin{aligned}
\mathrm{Re}\, E_{0+}^{\gamma \pi^0} = {} & \mathrm{Re}\, E_{0+}^{\gamma \pi^0}(\mathrm{IS}) \\
& - a_{\pi N}\, \omega_c\, \mathrm{Re}\, E_{0+}^{\gamma \pi^+}(\mathrm{IS}) \sqrt{1 - \frac{\omega^2}{\omega_c^2}},
\end{aligned} \tag{5}
$$

where ω and ω_c are the π^0 and π^+ c.m. energies corresponding to $E = E_p + E_\gamma$ and $m_n + m_{\pi^+}$, respectively, and $a_{\pi N} = 0.124/m_{\pi^+}$ is the pion charge ex-
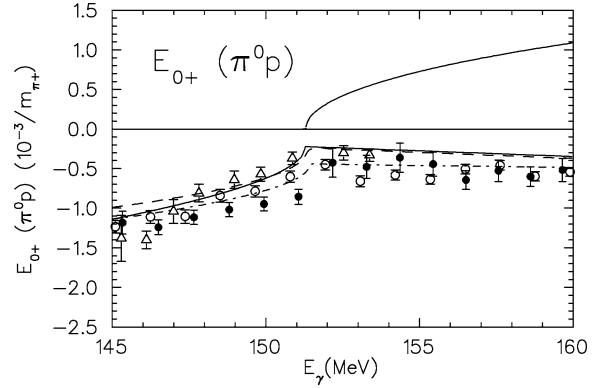
change threshold amplitude. $E_{0+}^{\gamma \pi^{0,+}}(\mathrm{IS})$ is the $\pi^{0,+}$ photoproduction amplitude obtained with the assumption of isospin symmetry (IS), i.e., without the pion mass difference in Eq. (3). Such an approximation is often used in the data analysis in order to parametrize the E_{0+} multipole below $\pi^+ n$ threshold in the form of $E_{0+}(E) = a + b \sqrt{1 - (\omega/\omega_c)^2}$. In Fig. 2 the results obtained from such an approximation scheme are represented by the solid curve and compared to the exact coupled channels (dashed curve) and ChPT calculations (dash-dotted curve) [9]. We see that above π^+ threshold the difference between the results obtained with physical and isospin bases is very small. This is consistent with the finding of Ref. [32]. At lower energies the difference becomes visible only very close to $\pi^0 p$ threshold where the two approaches differ by about 10%. In general we can conclude that the simple expression of Eq. (5) is a good approximation for the pion-mass difference effect, and in the following calculations we will use this option to analyze the experimental data. Note that the correct threshold dependence of the imaginary part can be obtained from the Fermi–Watson theorem if in the threshold region the πN phase shift is taken as a linear function of the π^+ momentum, i.e., vanishing as $q_{\pi^+} \to 0$.

In Fig. 3, we compare the predictions of our model for the differential cross section with recent photoproduction data from Mainz [3,8]. The dotted and solid
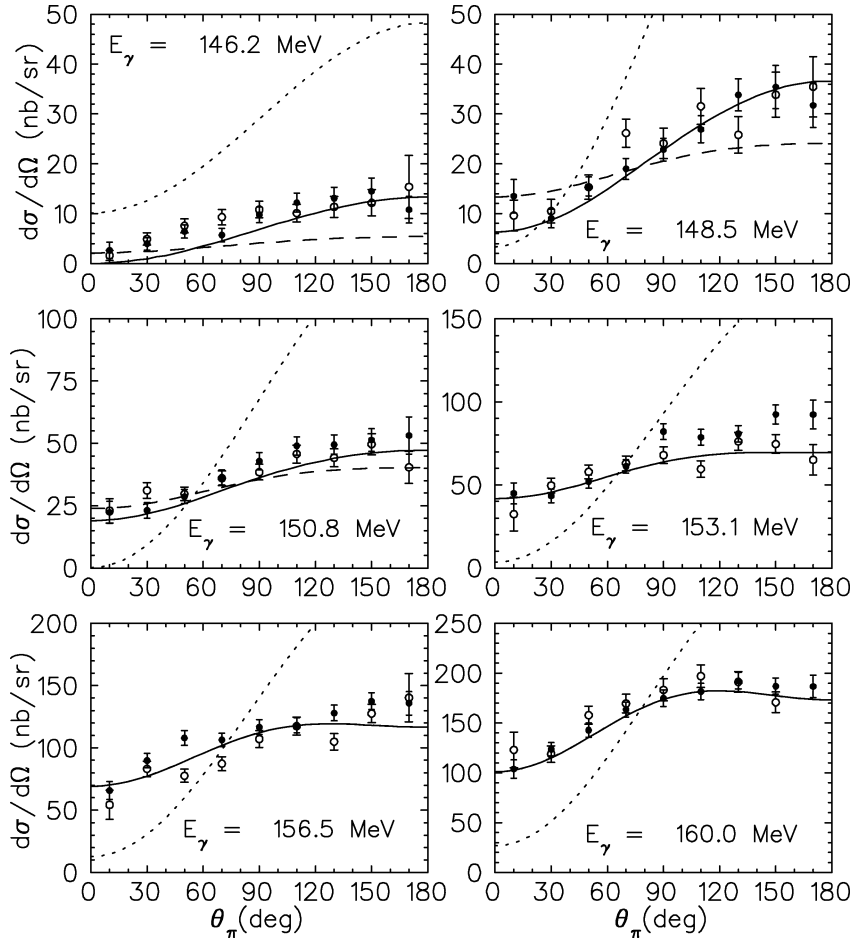
Fig. 3. Differential cross sections for $\gamma p \rightarrow \pi^0 p$. Dotted and dashed curves: the results obtained without and with FSI contributions using isospin symmetry. Solid curves: final result including pion mass difference effects. Experimental data from Ref. [3] (•) and Ref. [8] (○).

curves are obtained without and with FSI effects, respectively. It is seen that both off-shell pion rescattering and cusp effects substantially improve the agreement with the data. This indicates that our model gives reliable predictions also for the threshold behaviour of the P-waves without any additional arbitrary parameters. As an example, numerical values for E_{0+} (in units of $10^{-3}/m_{\pi^+}^3$) and P-wave multipoles (in units of $10^{-3}q/m_{\pi^+}^3$) at π^0 threshold are given in Table 1. For the P-wave multipoles we give values for the following linear combinations: $P_1 = 3E_{1+} + M_{1+} - M_{1-}$, $P_2 = 3E_{1+} - M_{1+} + M_{1-}$ and $P_3 = 2M_{1+} + M_{1-}$.

The contributions of Born terms, vector meson exchange, FSI and resonances ($S_{11}(1535)$, $\Delta(1232)$ and $P_{11}(1440)$) are listed in Table 1 to show their relative importance. One observes that ρ- and mostly ω-exchange give important contributions to the P-wave amplitudes, especially to P_3, where Born terms contribute only 2%. Half of P_3 comes from the vector meson exchanges and the rest from FSI and resonance contributions. Due to the large contribution from these three mechanisms, P_3 becomes comparable to P_1 and P_2. Very close to threshold, our model predicts $|P_3/P_2| \simeq 0.9$, and a small but negative value for the photon asymmetry $\Sigma(\theta_\pi = 90°) \sim |P_3|^2 - |P_2|^2$

Table 1

E_{0+} (in units $10^{-3}/m_{\pi^+}$) at threshold and P_1, P_2 and P_3 (in units $10^{-3}q/m_{\pi^+}^2$). Contributions of Born terms (Born), vector mesons ($\omega + \rho$), pion rescattering (FSI) and resonances (res.) are shown separately. The predictions of ChPT and recent experimental values are taken from Ref. [10] and Ref. [8]

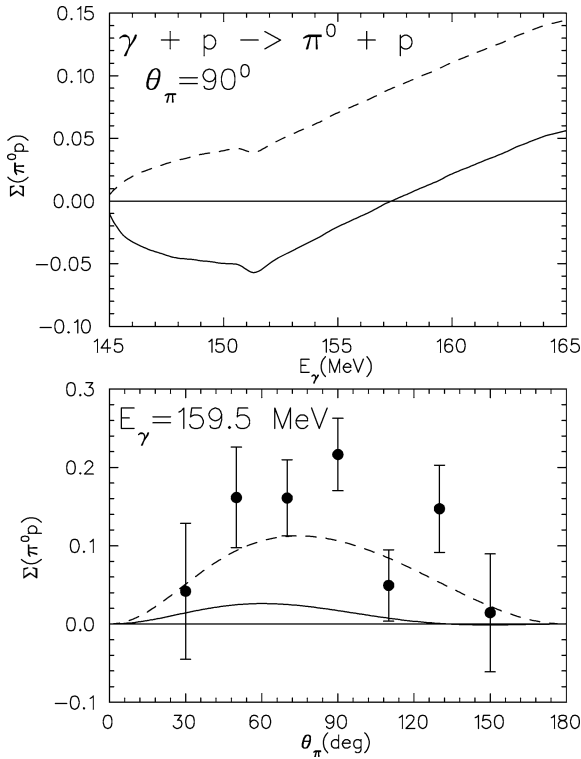|	Born	$\omega + \rho$	FSI	Res.	Tot.	ChPT	Exp.
E_{0+}	−2.46	0.17	1.06	0.07	−1.16	−1.16	−1.33 ± 0.11
P_1	9.12	−0.35	0.15	0.38	9.30	9.14	9.47 ± 0.37
P_2	−8.91	0.21	−1.32	−0.13	−10.15	−9.7	−9.46 ± 0.39
P_3	0.18	4.61	3.36	1.20	9.35	10.36	11.48 ± 0.41

Fig. 4. Solid curves are our predictions for the energy dependence of the photon asymmetry Σ at $\theta_\pi = 90°$ (upper panel) and its angular distribution at $E_\gamma = 159.5$ MeV (lower panel) in $\gamma p \rightarrow \pi^0 p$. Dashed curves are results obtained with a 15% reduction of the M_{1-} multipole in the model. Experimental data from Ref. [8].

at fixed pion c.m. angle $\theta_\pi = 90°$. As shown by the solid curve in Fig. 4, our prediction for $\Sigma(\theta_\pi = 90°)$ first tends to more negative values before bending over and becoming positive at large photon energies. It was found in Ref. [33] that in the threshold region this ob-

servable is very sensitive to the M_{1-} multipole which strongly depends on the details of the low energy behavior of Roper resonance, vector meson and FSI contributions. Therefore, a slight modification of one or all of these mechanisms can drastically change the photon asymmetry. As an illustration, our prediction for the energy dependence and angular distribution of $\Sigma(\theta_\pi)$ obtained with a 15% reduction of the M_{1-} multipole, is shown by dashed curves in Fig. 4. This small modification of the low energy tail of the Roper resonance leads to positive photon asymmetries at all energies!

In Table 1, the ChPT predictions and the experimental values extracted from recent TAPS polarization measurements [8] are listed for comparison. Our predictions are in good overall agreement with the ChPT predictions [10] and the TAPS results. However, there is a 15–20% difference in P_3 which leads to an underestimation of our result for the photon asymmetry, as shown in Fig. 4. Note that, in contrast to our model, P_3 is essentially determined by a low energy constant in ChPT.

Pion electroproduction provides us with information on the $Q^2 = -k^2$ dependence of the transverse E_{0+} and longitudinal L_{0+} multipoles in the threshold region. The "cusp" effects in the L_{0+} multipole is taken into account in a similar way as in the case of E_{0+},

$$\text{Re}\, L_{0+}^{\gamma\pi^0} = \text{Re}\, L_{0+}^{\gamma\pi^0}\,(\text{IS})$$

$$- a_{\pi N}\omega_c\, \text{Re}\, L_{0+}^{\gamma\pi^+}\,(\text{IS})\sqrt{1 - \frac{\omega^2}{\omega_c^2}}, \qquad (6)$$

where all the multipoles are functions of total c.m. energy E and virtual photon four-momentum squa-

Table 2
Comparison of the S- and P-wave multipoles (in units $10^{-3}/m_{\pi+}$) for the $p(\gamma^*, \pi^0)p$ reaction at $Q^2 = 0$, 0.05 and 0.10 $(\text{GeV}/c)^2$, obtained in our model and ChPT [10] at $\Delta W = 2.5$ MeV

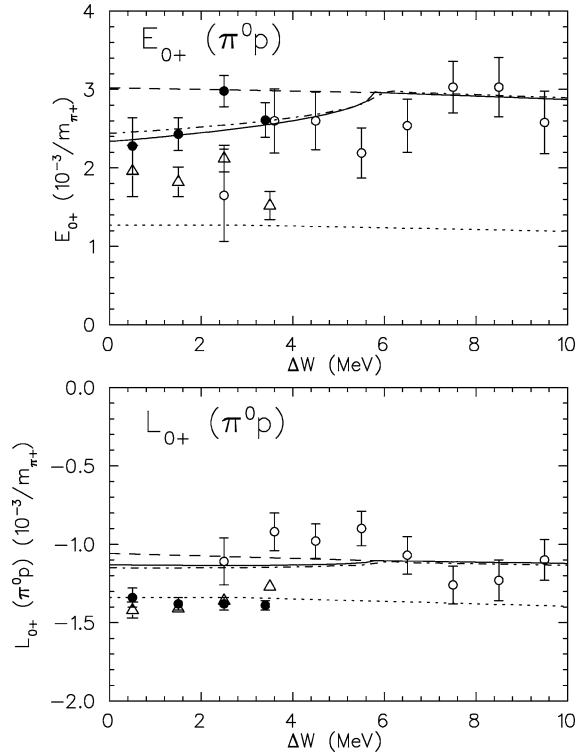| Q^2 $(\text{GeV}/c)^2$	0.0	0.0	0.05	0.05	0.1	0.1
Model	DM	ChPT	DM	ChPT	DM	ChPT
E_{0+}	−0.92	−0.96	1.08	0.45	2.48	1.60
M_{1+}	1.11	1.19	1.70	2.16	1.93	2.74
M_{1-}	−0.59	−0.49	−0.96	−0.72	−1.07	−0.74
E_{1+}	−0.02	−0.02	−0.03	−0.01	−0.03	−0.01
L_{0+}	−2.71	−1.61	−1.74	−1.52	−1.13	−1.31
L_{1-}	−0.14	−0.52	−0.05	−0.60	−0.01	−0.51
L_{1+}	−0.01	−0.01	−0.01	−0.02	−0.01	−0.02

Fig. 5. Real parts of E_{0+} (upper panel) and L_{0+} (lower panel) for $ep \rightarrow e'\pi^0 p$ at $Q^2 = 0.1$ $(\text{GeV}/c)^2$. Dash-dotted curves are the results of full calculations obtained using Eq. (4) without the assumption of isospin symmetry. Notations for other curves are the same as in Fig. 3. Data points from Ref. [5] (○) and Ref. [6] (△). The results of the present work obtained by using the P-waves of our model are given by (●).

red Q^2. It is known that at threshold, the Q^2 dependence is given mainly by the Born plus vector meson contributions in $v_{\gamma\pi}^B$, as described in Ref. [30].

The validity of the approximation made in Eq. (6) is confirmed in Fig. 5 where the results of K-matrix approximation (solid lines) and full calculation (dash-dotted lines) agree with each other within a few percent. In Fig. 5 we also show our results for the cusp and FSI effects in the E_{0+} and L_{0+} multipoles for π^0 electroproduction at $Q^2 = 0.1$ $(\text{GeV}/c)^2$, along with the results of the multipole analysis from NIKHEF [5] and Mainz [6]. Note that results of both groups were obtained using the P-wave predictions given by ChPT. However, there exist substantial differences between the P-wave predictions of ChPT and our model at finite Q^2, as presented in Table 2. To understand the consequence of these differences, we have made a new analysis of the Mainz data [6] for the differential cross sections, using our DM prediction for the P-wave multipoles instead. The S-wave multipoles extracted this way are also shown in Fig. 5 by solid circles and listed in Table 3. We see that the results of such a new analysis gives a E_{0+} multipole closer to the NIKHEF data and in better agreement with our dynamical model prediction. However, the results of our new analysis for the longitudinal L_{0+} multipole stay practically unchanged from the values found in the previous analyses. Note that the dynamical model prediction for L_{0+} again agrees much better with the NIKHEF data.

Table 3
Values of the E_{0+} and L_{0+} (in units $10^{-3}/m_{\pi^+}$) for the $p(\gamma^*, \pi^0)p$ reaction at $Q^2 = 0.10$ (GeV/c)^2, obtained after the local fit to the differential cross sections measured in Ref. [6]

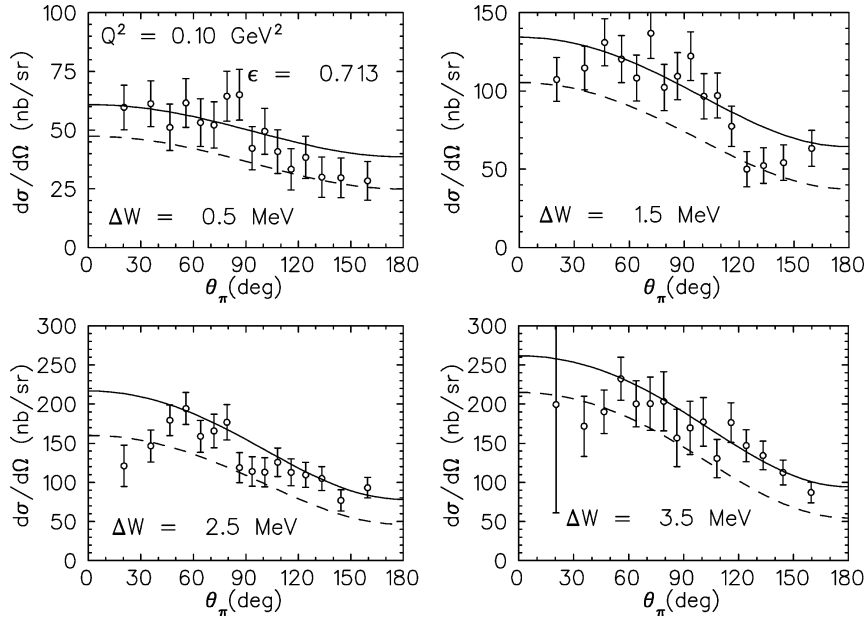| ΔW	E_{0+}	L_{0+}	χ^2/d.o.f.
0.5 Ref. [6]	2.28 ± 0.36	-1.34 ± 0.06	1.49
	1.96 ± 0.33	-1.42 ± 0.05	1.29
1.5 Ref. [6]	2.43 ± 0.21	-1.38 ± 0.04	1.26
	1.82 ± 0.19	-1.41 ± 0.03	1.19
2.5 Ref. [6]	2.98 ± 0.20	-1.38 ± 0.04	1.60
	2.12 ± 0.17	-1.36 ± 0.05	1.68
3.5 Ref. [6]	2.61 ± 0.22	-1.39 ± 0.03	1.70
	1.52 ± 0.18	-1.27 ± 0.03	1.84

Fig. 6. Angular distribution $d\sigma/d\Omega = d\sigma_T/d\Omega + \epsilon \, \sigma_L/d\Omega$ for $ep \rightarrow e'\pi^0 p$ at $Q^2 = 0.1$ (GeV/c)^2 and $\epsilon = 0.713$, at different total c.m. energies $\Delta W = W - W_{\text{thr}}^{\pi^0 p}$. Dashed curves are predictions of our model. Solid curves are the results of our local fit with fixed P-waves. Experimental data from Ref. [6].

In Figs. 6 and 7, our model predictions (dashed curves) are compared with the Mainz experimental data [6] for the unpolarized cross sections $d\sigma/d\Omega = d\sigma_T/d\Omega + \epsilon \, d\sigma_L/d\Omega$, and for the longitudinal-transverse cross section $d\sigma_{TL}/d\Omega$. Overall, the agreement is good. The solid curves are the results of our best fit at fixed energies (local fit) obtained by varying only the E_{0+} and L_{0+} multipoles. We have found that the differences between the solid and dashed curves in Figs. 6 and 7 are mostly due to the difference in the L_{0+} multipole (see also Fig. 5).

Finally we discuss a new version (hereafter called MAID) [34] of the unitary isobar model developed at Mainz (hereafter called MAID98) [30], which is cur-
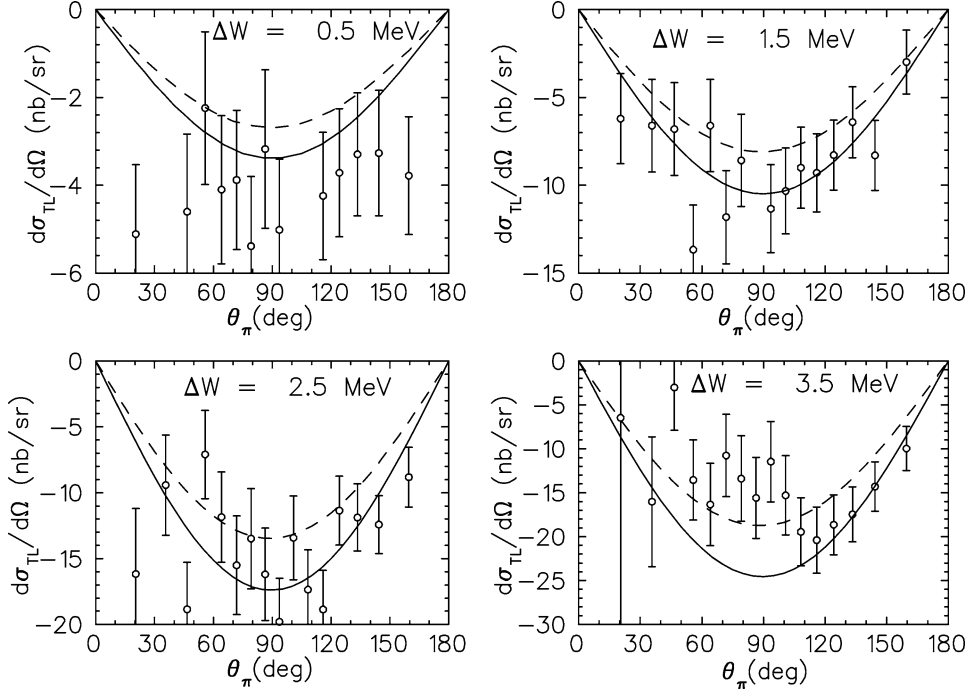
Fig. 7. Same as in Fig. 6 for the transverse-longitudinal cross section $d\sigma_{TL}/d\Omega$.

rently being intensively used for the analysis of pion photo- and electroproduction data. In this model the FSI effects are taken into account using the K-matrix approximation, namely without the inclusion of off-shell pion rescattering contributions (principal value integral) in Eq. (3). As a result, the S-, P-, D- and F-waves of the background contributions are defined in MAID as

$$t_\alpha^B(\text{MAID}) = \exp(i\delta_\alpha)\cos\delta_\alpha\, v_\alpha^B(q_E, k). \qquad (7)$$

However, as we have found above, dynamical model calculations show that pion off-shell rescattering is very important at low pion energies. The prediction of MAID for π^0 photoproduction at threshold, represented by the dotted curves in Figs. 1 and 2, lies substantially below the data. It turns out that it is possible to improve MAID, in the case of π^0 production at low energies, by introducing a phenomenological term and including the cusp effect of Eq. (5). In this extended version of MAID, we write the $E_{0+}(\pi^0 p)$ multipole

as

$$\text{Re}\, E_{0+}^{\gamma\pi^0} = \text{Re}\, E_{0+}^{\gamma\pi^0}(\text{MAID98}) + E_{\text{cusp}}(W, Q^2)$$
$$+ E_{\text{corr}}(W, Q^2), \qquad (8)$$

where

$$E_{\text{cusp}} = -a_{\pi N}\omega_c \, \text{Re}\, E_{0+}^{\gamma\pi^+}(\text{MAID98}) \sqrt{1 - \frac{\omega^2}{\omega_c^2}}. \qquad (9)$$

The phenomenological term E_{corr} which emulates the pion off-shell rescattering corrections (or pion-loop contribution in ChPT) can be parameterized in the form

$$E_{\text{corr}}(W, Q^2) = \frac{A}{(1 + B^2 q_\pi^2)^2} F_D(Q^2), \qquad (10)$$

where F_D is the standard nucleon dipole form factor. The parameters A and B are obtained by fitting to the low energy π^0 photoproduction data: $A = 2.01 \times 10^{-3}/m_{\pi^+}$ and $B = 0.71$ fm.

In summary, we have shown that within a meson-exchange dynamical model [25], one is able to describe photo- and electroproduction in the threshold

region in good agreement with the data. The model has been demonstrated [34,35] to give a good description of most of the existing pion electromagnetic production data up to the second resonance region. The success of such a model at intermediate energies is perhaps not surprising since unitarity plays an important role there. However, it is not a priori clear that our model should also work well near threshold, even though we do start from an effective chiral Lagrangian. In principle, crossing symmetry is violated and the well-defined power counting scheme in ChPT is lost by rescatterings. As a matter of fact, previous similar attempts have failed [22,24]. It is easy to understand the difference between our present calculation and the results of Ref. [22] by the fact that the off-shell behavior of the πN models used [13] are quite different from each other. The difference between our results and those of Ref. [24] probably arises, in large part, from different off-shell prescriptions used for the transition potential $v_{\gamma\pi}$, because the meson-exchange πN model used in Ref. [24] is very similar to the one used in this study. On the other hand, meson-exchange models [16,17] have also been shown to give a good description of low energy πN data, in addition to an excellent agreement with the data at higher energies. It is, therefore, assuring that similar success can also be achieved for the pion electromagnetic production.

The largest discrepancy between our results and the data is in the P_3 amplitude where our prediction underestimates the data by about 20%. As a consequence, our prediction for the photon asymmetry has the opposite sign as observed in the experiment [8]. However, we have found that in the threshold region, the photon asymmetry is very sensitive to many ingredients of the theory, e.g., vector mesons, FSI and Roper resonance contributions, a fact that deserves further studies.

Finally, we found that the effects of final state interaction in the threshold region and in the case of π^0 production, are nearly saturated by the single rescattering term. Therefore, the existing one-loop calculations in ChPT could be a good approximation to threshold neutral pion production.

Acknowledgements

References

[1] See, e.g., in: A.M. Bernstein, D. Drechsel, Th. Walcher (Eds.), Chiral Dynamics: Theory and Experiment, Springer-Verlag, Berlin, 1998.
[2] R. Beck et al., Phys. Rev. Lett. 65 (1990) 1841.
[3] M. Fuchs et al., Phys. Lett. B 368 (1996) 20.
[4] J.C. Bergstrom et al., Phys. Rev. C 53 (1996) R1052;
J.C. Bergstrom et al., Phys. Rev. C 55 (1997) 2016.
[5] H.B. van den Brink et al., Phys. Rev. Lett. 74 (1995) 3561;
H.B. van den Brink et al., Nucl. Phys. A 612 (1997) 391.
[6] M.O. Distler et al., Phys. Rev. Lett. 80 (1998) 2294.
[7] A.M. Bernstein et al., Phys. Rev. C 55 (1997) 1509.
[8] A. Schmidt et al., nucl-ex/0105010.
[9] V. Bernard, J. Gasser, N. Kaiser, U.-G. Meißner, Phys. Lett. B 268 (1991) 291.
[10] V. Bernard, N. Kaiser, U.-G. Meißner, Z. Phys. C 70 (1996) 483;
V. Bernard, N. Kaiser, U.-G. Meißner, Nucl. Phys. A 607 (1996) 379, and references contained therein.
[11] B.C. Pearce, B.K. Jennings, Nucl. Phys. A 528 (1991) 655.
[12] C.C. Lee, S.N. Yang, T.-S.H. Lee, J. Phys. G 17 (1991) L131.
[13] C.T. Hung, S.N. Yang, T.-S.H. Lee, J. Phys. G 20 (1994) 1531;
C.T. Hung, S.N. Yang, T.-S.H. Lee, Phys. Rev. C 64 (2001) 034309.
[14] F. Gross, Y. Surya, Phys. Rev. C 47 (1993) 703;
F. Gross, Y. Surya, Phys. Rev. C 53 (1996) 2422.
[15] T. Sato, T.-S.H. Lee, Phys. Rev. C 54 (1996) 2660.
[16] A.D. Lahiff, I.R. Afnan, Phys. Rev. C 60 (1999) 024608.
[17] V. Pascalutsa, J.A. Tjon, Phys. Rev. C 61 (2000) 054003.
[18] S. Nozawa, B. Blankleider, T.-S.H. Lee, Nucl. Phys. A 513 (1990) 459;
S. Nozawa, T.-S. Lee, Nucl. Phys. A 513 (1990) 511.
[19] S.N. Yang, Chin. J. Phys. 29 (1991) 485.
[20] S.S. Hsiao, C.T. Hung, J.L. Tsai, S.N. Yang, Y.-B. Dong, Few Body Systems 25 (1998) 55.
[21] Y. Surya, F. Gross, Phys. Rev. C 53 (1996) 2422.
[22] S.N. Yang, Phys. Rev. C 40 (1989) 1810.
[23] S. Nozawa, T.-S.H. Lee, B. Blankleider, Phys. Rev. C 41 (1990) 213.
[24] T.-S.H. Lee, B.C. Pearce, Nucl. Phys. A 530 (1991) 532.
[25] S.S. Kamalov, S.N. Yang, Phys. Rev. Lett. 83 (1999) 4494.
[26] H. Tanabe, K. Ohta, Phys. Rev. C 31 (1985) 1876.
[27] S.N. Yang, J. Phys. G 11 (1985) L205.
[28] M. Cooper, B. Jennings, Nucl. Phys. A 500 (1989) 553.
[29] M.G. Olsson, E.T. Osypowsky, Nucl. Phys. B 87 (1975) 399.

[30] D. Drechsel, O. Hanstein, S.S. Kamalov, L. Tiator, Nucl. Phys. A 645 (1999) 145.

[31] A.M. Bernstein, Phys. Lett. B 442 (1998) 20.

[32] J.M. Laget, Phys. Rep. 69 (1981) 1.

[33] O. Hanstein, D. Drechsel, L. Tiator, Phys. Lett. B 385 (1996) 45;
O. Hanstein, D. Drechsel, L. Tiator, Nucl. Phys. A 632 (1998) 561.

[34] S.N. Yang, G.Y. Chen, S.S. Kamalov, D. Drechsel, L. Tiator, Invited talk presented at the NSTAR2001 workshop, March 6–10, 2001, Mainz, to be published by World Scientific, Singapore, 2001, nucl-th/0106027.

[35] S.S. Kamalov, D. Drechsel, L. Tiator, S.N. Yang, N^*2001 Workshop (s.a.), nucl-th/0106045.